

Supplementary material

Dominance of tectonics over climate in Himalayan denudation

Vincent Godard, Didier L. Boursès, Françoise Spinabella, Douglas W. Burbank, Bodo Bookhagen, G. Burch Fisher, Adrien Moulin, Laëtitia Léanni

All analytical results are listed in table DR1 and geomorphological parameters associated with the catchments are presented in table DR2. Five additional samples used in this analysis are taken from Godard et al. [2012].

Analytical procedure

Chemical preparation and Be isolation

Bulk sand samples were sieved to extract the 250-1000 μ m fraction, which was submitted to sequential magnetic separation. The remaining fraction was leached with 37% HCl to remove carbonate fragments. The samples were then repetitively leached with H₂SiF₆ and submitted to vigorous mechanical shaking until pure quartz was obtained. Decontamination from atmospheric ¹⁰Be was achieved by a series of three successive leaching in concentrated HF (each leaching removing 10% of the remaining sample mass) [Brown et al., 1991]. After addition of a ⁹Be carrier (\sim 100 μ l at 3.025 x 10⁻³ g/g) the samples were digested in concentrated HF and Be was isolated for measurements using ion-exchange chromatography.

AMS measurements

¹⁰Be measurements were performed by M. Arnold, G. Aumaître and K. Keddadouche at the French AMS National Facility, ASTER, located at CEREGE in Aix-en-Provence. This instrument is supported by the INSU/CNRS, the French Ministry of Research and Higher Education, IRD and CEA. ¹⁰Be data were calibrated directly against the National Institute of Standards and Technology standard reference material 4325 by using an assigned value of $(2.79\pm 0.03)\times 10^{-11}$ [Nishiizumi et al., 2007].

Uncertainties

Uncertainties on ¹⁰Be concentrations (reported as 1 σ) are calculated according to the standard error propagation method using the quadratic sum of the relative errors and include a conservative 0.5% external machine uncertainty [Arnold et al., 2010], a 1.08% uncertainty on the certified standard ratio, a 1 σ uncertainty associated to the mean of the standard ratio measurements during the measurement cycles, a 1 σ statistical error on counted ¹⁰Be events and the uncertainty associated with the chemical and analytical blank correction. An additional uncertainty of 10% was assumed for the production rate calculation and included in the total uncertainty on the denudation rate.

Process blanks

Five process blanks were treated and measured along with our samples, yielding ¹⁰Be/⁹Be ratios of 1.17 \pm 0.44, 1.33 \pm 0.32, 1.36 \pm 0.33, 0.76 \pm 0.43 and 1.34 \pm 0.59 $\times 10^{-15}$. It corresponds to an upper 1 σ bound of 25 to 40 $\times 10^3$ ¹⁰Be atoms for the background level in our blanks, which is at least one order of magnitude lower than the number of ¹⁰Be atoms in the dissolved sample masses.

Naturally occurring ⁹Be

In order to test the possibility that ⁹Be could be significantly present in our samples (in addition of that provided by the carrier solution), we digested \sim 2 g of pure quartz for 29 of our samples (using the same purified and leached fraction that was used for the main samples) and measured the Be concentration by ICP-OES. The average concentration is 48 ppb, with a maximum of 229 ppb (sample KP-090311-06). Once the carrier solution is added natural ⁹Be represents in average 0.3% of all ⁹Be present in the digested sample (1.5% for sample KP-090311-06). Accounting for the presence of this natural ⁹Be only changes the calculated ¹⁰Be concentration by 0.3% on average, and by 1.5% when considering the maximum ⁹Be concentration obtained for sample KP-090311-06.

GIS analysis

All our topographic analyses are based on a hole-filled 90-m SRTM DEM¹.

Production and erosion rates calculations

Production rates were calculated using the approach of Stone [2000] at each pixel of the 90-m resolution DEM. We use 4.5 at/g/yr as the sea-level high latitude production rate for ¹⁰Be [Nishiizumi et al., 2007]. Topographic shielding was calculated at each pixel of the DEM following the method of Dunne et al. [1999].

In all calculations, we use 2.65 g/cm³ for the density for quartz and attenuation lengths from Braucher et al. [2003, 2011] : 160, 1500 and 4320 g/cm² for neutrons, slow and fast muons respectively.

Steepness indexes calculation

We have calculated channel steepness following standard procedures [Wobus et al., 2006] and we have normalized the channel steepness index (ksn) with a reference concavity of 0.45 [Whipple and Tucker, 1999]. Concavity measurements from a nearby area in the western Himalaya indicates that the theoretical steepness index of 0.45 is very close to the measured values (0.43 ± 0.12 , Scherler et al. [2013, in press]). Channel steepness indices were taken from smoothed 1-km-long channel reaches (i.e., smoothing over ~ 11 grid points). Since very few of our studied catchments show signs of glaciations, the reference concavity of ~ 0.45 is a very valid assumption [Scherler et al., 2013, in press]. There exist some knickpoints in the study area, that are mostly located along major trans-himalayan rivers, and are related to major tectonics units [Seeber and Gornitz, 1983].

¹Jarvis, A., H.I. Reuter, A. Nelson, E. Guevara, 2008, Hole-filled SRTM for the globe Version 4, available from the CGIAR-CSI SRTM 90m Database (<http://srtm.csi.cgiar.org>)

Sample	Lon.	Lat.	Mass ¹ [g]	[¹⁰ Be] ×10 ³ at/g	N ³ _{spal}	Shield. ⁴	Denud. rate [mm/yr]	Time scale ⁵ [yr]
KP-090311-01	85.0659	27.74690	20.5	41.91±2.89	2.6	0.93	0.19±0.02	3194
KP-090311-02	84.9673	27.80740	21.0	25.09±2.47	1.7	0.95	0.21±0.03	2811
KP-090311-03	84.9506	27.81133	22.7	35.01±2.40	2.2	0.94	0.20±0.02	3057
KP-090311-04	84.8893	27.80535	18.6	27.10±2.39	1.8	0.94	0.21±0.03	2922
KP-090311-05	84.8336	27.80310	20.5	17.14±2.36	2.0	0.92	0.36±0.06	1662
KP-090311-06	84.7514	27.80117	20.0	10.63±1.49	1.7	0.92	0.49±0.08	1227
KP-090311-07	84.6938	27.80455	9.7	24.96±3.28	2.0	0.91	0.24±0.04	2524
KP-090311-08	84.6338	27.87164	20.7	11.10±1.17	1.7	0.95	0.49±0.07	1224
KP-160311-09	84.0604	28.06691	20.3	41.61±2.63	1.6	0.95	0.13±0.01	4829
KP-160311-10	84.0781	28.01293	18.2	38.68±2.60	1.6	0.95	0.14±0.02	4435
KP-160311-11	84.2389	27.98867	20.0	44.02±2.31	1.4	0.96	0.10±0.01	5763
KP-160311-12	84.2637	28.02910	19.3	47.81±3.41	1.4	0.96	0.10±0.01	6259
PO-140311-01	83.7725	28.31098	19.3	22.40±2.23	4.9	0.91	0.63±0.09	958
PO-150311-02	83.7355	28.27546	20.3	11.78±1.61	3.5	0.91	0.88±0.15	692
PO-150311-03a	83.7149	28.23183	19.5	10.48±1.67	2.7	0.95	0.78±0.15	768
PO-150311-05	83.6132	28.25353	20.2	34.55±3.07	3.0	0.93	0.26±0.04	2284
TR-170311-01	85.1358	27.92143	18.9	12.91±2.20	2.2	0.93	0.52±0.10	1155
TR-170311-02	85.1907	27.97581	20.1	15.07±2.35	4.5	0.90	0.85±0.16	714
TR-170311-03	85.1756	27.98276	20.0	8.15±1.11	3.7	0.92	1.33±0.22	454
TR-170311-04	85.1541	27.86571	20.7	29.14±2.68	2.0	0.93	0.22±0.03	2786
EK-180311-01	85.6173	27.64413	21.3	58.58±3.00	2.2	0.96	0.12±0.01	845
EK-180311-02	85.7347	27.67731	22.9	64.59±2.89	2.6	0.94	0.12±0.01	4848
EK-180311-03	85.8597	27.75320	19.5	12.84±1.80	3.1	0.92	0.71±0.12	845
EK-180311-04	85.8961	27.77829	20.8	11.92±2.87	4.5	0.88	1.05±0.27	574
EK-180311-05	85.9152	27.88193	21.8	10.12±2.54	6.5	0.91	1.81±0.49	334

Table DR1: Analytical results associated with the samples processed in this study. All reported uncertainties are $\pm 1\sigma$. See text for details on the sample processing and data treatment. ¹ Mass of pure quartz dissolved. ³ Catchment averaged spallation production rate scaling factor for latitude and elevation according to Stone [2000, equation 2]. ⁴ Catchment averaged topographic shielding calculated from Dunne et al. [1999]. See Godard et al. [2012] for analytical details of the five samples from the Marsyandi catchment. ⁵ Integration time-scale for denudation.

Sample	Elevation ¹ [km]	Area [km ²]	Slope [°]	Precip. ² [m/yr]	Rock Uplift ³ [mm/yr]	SSPW ⁴ [W/m ²]	ks _n [m ^{0.9}]	Relief ⁵ [km]
Samples from this study								
KP-090311-01	1.49 (0.62-2.49)	110.8	23.8	2.5	0.5	85.6	123.5	1.14-1.62
KP-090311-02	0.91 (0.46-1.62)	11.9	20.9	2.8	0.5	61.4	358.7	0.88-1.33
KP-090311-03	1.25 (0.41-2.33)	87.9	21.9	3.2	0.5	107.6	100	1.06-1.53
KP-090311-04	0.96 (0.4-1.97)	19.5	21.8	3.2	0.5	78.3	99.7	0.98-1.46
KP-090311-05	1.12 (0.37-2.34)	99.1	24.6	3.7	1	99.2	116.8	1.08-1.47
KP-090311-06	0.9 (0.33-1.86)	46.3	26.1	4.7	1.1	109.8	110.3	0.99-1.35
KP-090311-07	1.1 (0.32-1.92)	55.4	27.9	4.6	1.2	153.7	103.7	1.21-1.53
KP-090311-08	0.92 (0.28-1.59)	26.6	20.6	1.6	0.5	57.3	143.9	1.05-1.38
KP-160311-09	0.86 (0.5-1.56)	93.2	19.7	3.1	0.5	46.3	125.8	0.71-0.88
KP-160311-10	0.87 (0.45-1.55)	97	19.6	2.4	0.5	52.8	76.2	0.75-0.95
KP-160311-11	0.68 (0.33-1.26)	65.9	18.6	2.4	0.5	45.4	57.9	0.65-0.82
KP-160311-12	0.68 (0.36-1.2)	42.5	17.8	2.4	0.5	34.1	67.4	0.75-0.96
EK-180311-01	1.24 (0.85-2.04)	42.5	16.7	1.6	0.5	30.5	84.8	0.76-1.12
EK-180311-02	1.52 (0.66-2.25)	41.5	23	2.1	0.5	90.7	110	1.09-1.52
EK-180311-03	1.73 (0.78-2.75)	30.1	26	3.4	0.6	139.3	234	1.25-1.89
EK-180311-04	2.22 (0.86-3.75)	90.7	30.4	4.1	2.7	200.8	179.8	1.79-2.47
EK-180311-05	2.85 (1.23-4.29)	67.4	26.7	4.3	7.1	249.9	613.6	1.56-2.31
TR-170311-01	1.24 (0.54-2.46)	54.1	23.9	2.9	0.8	79.5	240.2	1.17-1.58
TR-170311-02	2.14 (0.63-4.54)	146.8	28.1	3.5	6	211.6	296.3	1.63-2.44
TR-170311-03	1.92 (0.64-3.61)	86.2	26.3	3	4.3	165.3	377.9	1.56-2.34
TR-170311-04	1.15 (0.54-2.05)	29.8	22.8	1.7	0.5	52.1	49.2	1.16-1.55
PO-140311-01	2.4 (1.06-3.59)	87.1	26.5	2.6	4.4	150.5	505.6	1.45-2.09
PO-150311-02	1.9 (0.89-3.16)	40.8	26.5	2.7	1	120.5	277.6	1.46-2.07
PO-150311-03a	1.52 (0.78-2.49)	40.8	19.4	3	0.8	108.9	244.9	1.1-1.56
PO-150311-05	1.71 (0.76-2.8)	116.5	23.8	2.4	0.5	107.5	158.6	1.27-1.73
Samples from Godard et al. (2012)*								
NEP003	1.48 (0.3-5.93)	608.6	23.1	2.2	3.3	116.2	183.4	1.22-1.77
NEP030	0.73 (0.38-1.63)	103.9	16.4	1.9	0.5	33	42.7	0.7-0.92
NEP080	1.82 (0.45-4.96)	309.3	22.8	2.7	4.9	141.7	247.3	1.33-1.99
NEP099	0.96 (0.52-1.89)	83	19.2	2.7	1.3	48.1	166.5	0.86-1.14
NIB-975-02	2.61 (0.81-4.96)	135.5	28	3.5	7.2	266.2	435.8	1.72-2.58

Table DR2: Geomorphological parameters associated with the studied catchments. ¹ Mean, min and max catchment elevation. ² Catchment averaged precipitation from Bookhagen and Burbank [2010]. ³ Catchment averaged rock uplift from Lavé and Avouac [2001]. ⁴ Catchment averaged specific stream power calculated using the scaling relationship between channel width W and discharge Q proposed by Burbank et al. [2003] : $W = 0.01Q^{0.4}$. ⁵ Reported values correspond to local relief calculated using moving windows of 5 and 10 km diameters. The typical length-scale of ridges spacing in our working area is comprised around 5 km. * The material for the sample NIB-975-02 was collected during the study of Brewer et al. [2006]. Most of the studied catchments are unglaciated and did not host any glaciers over the last climatic cycles. The Darondi catchment (NEP003, see Godard et al. [2012]) has a very small amount of his area glaciated in its headwaters (less than 1%), that is unlikely to impact its present day denudation, as seen through CRN. Some of the samples from basins inside the Marsyandi catchment (taken from Godard et al. [2012]) had small glaciers in their headwaters during the Last Glacial Maximum [Pratt-Sitaula et al., 2011], but that did not results in a significant glacial imprint, and this is again unlikely to affect modern denudation.

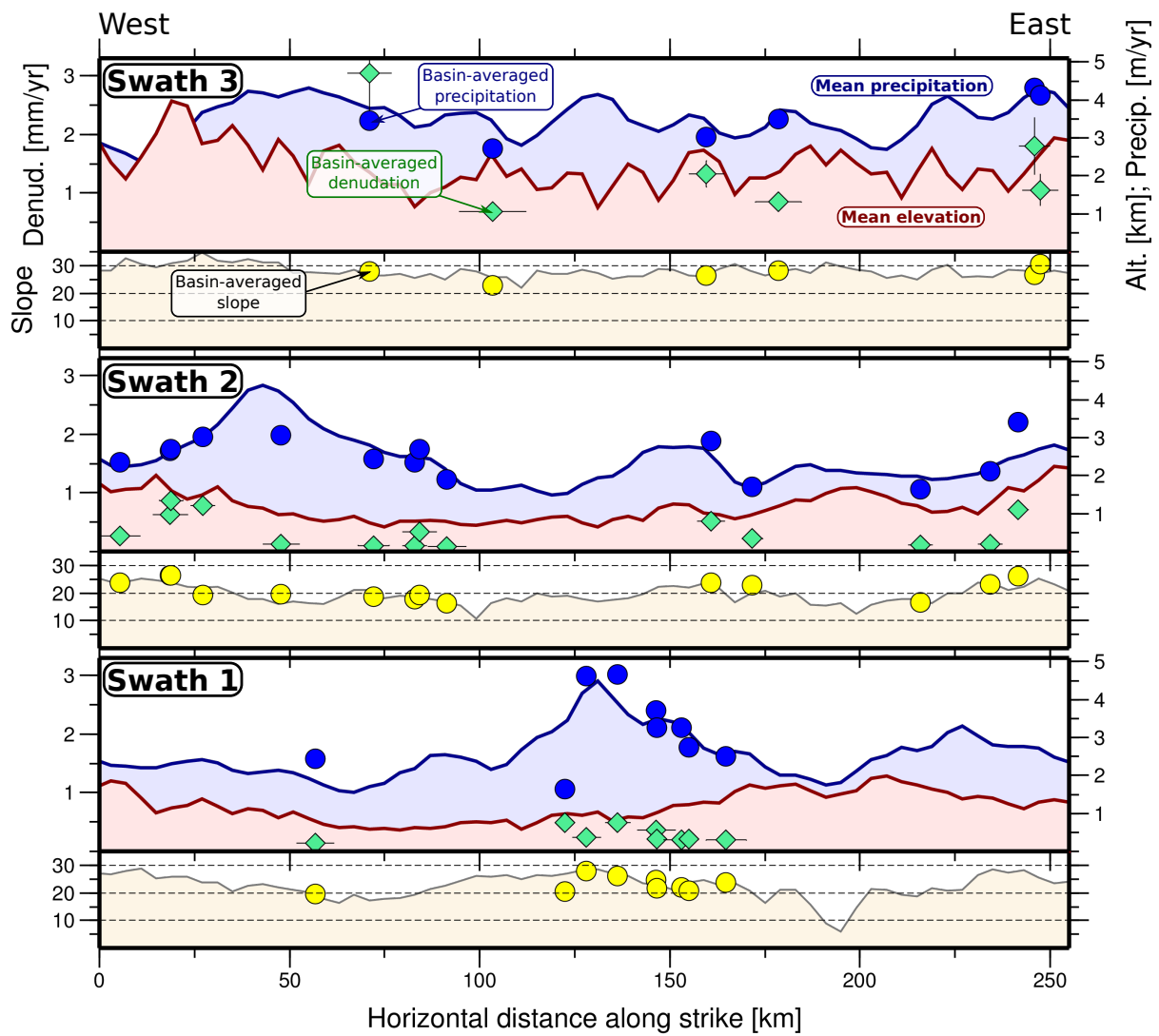


Figure DR1: Along-strike profiles (see Fig. 1 in the main text for location and extent of the swaths). Green diamonds are basin-averaged denudation rates. Error bars on denudation rates are $\pm 1\sigma$ and error bars on distance along-strike correspond to the square root of basin area. Blue and red curves are averaged elevation and precipitation [Bookhagen and Burbank, 2010] along the swath profiles. Blue circles are average precipitation values over the studied basins. Grey curve is hillslope angle averaged along the swath profiles. Yellow circles are average hillslope angles over the studied basins. Consideration of the variations of precipitation and denudation along strike allows these data to be separated into groups with similar rock uplift rates. For all three east-west sub-regions, the fluctuations of precipitation and denudation along strike appear mostly uncorrelated. Notably, in the swath 3 (southern), while from 125 km to 160 km precipitation decreases from 4.5 down to 2.5 m/yr, only subtle variations in denudation rates are observed. This lack of correlation strongly suggests a dominant control of tectonics, rather than climate, in dictating the pattern of denudation.

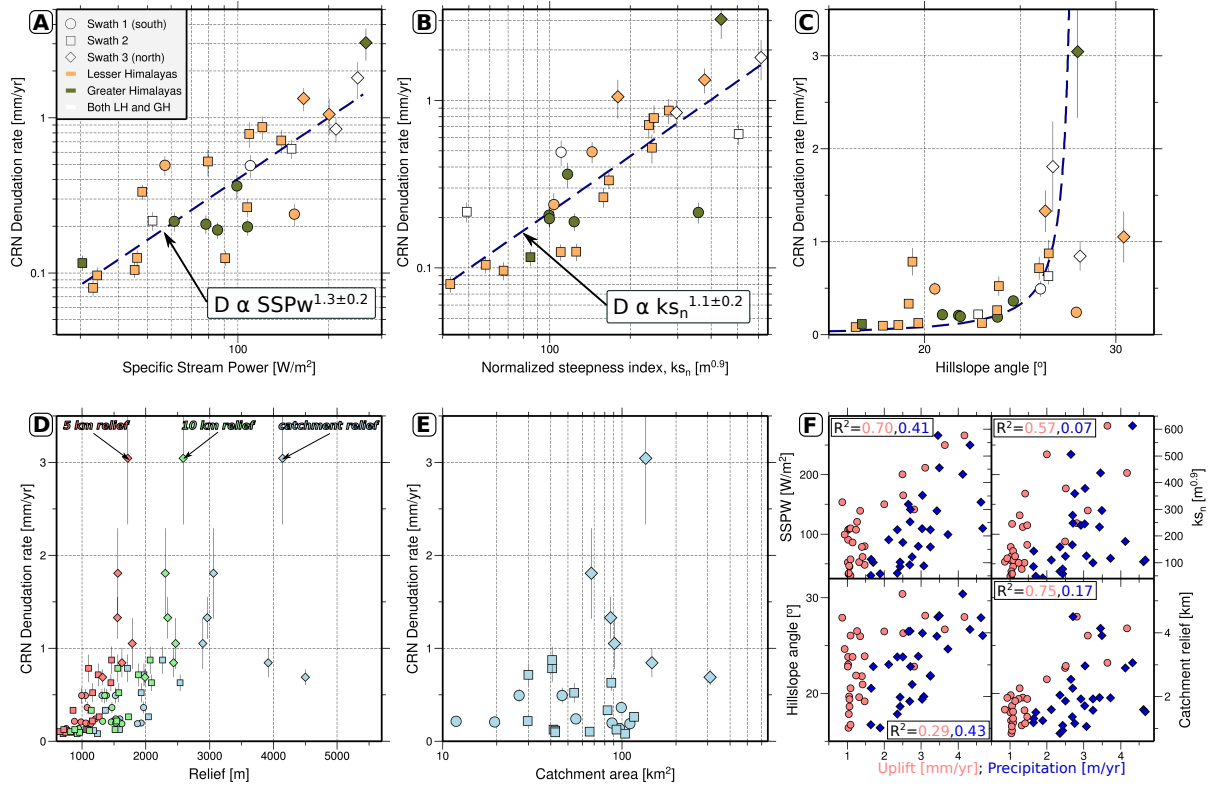


Figure DR2: (A) Comparison between basin-averaged denudation rate and specific stream power, showing a positive, slightly non-linear relationship between the two parameters with a power law exponent similar to that proposed by Bookhagen and Strecker [2012]. Channel width W is scaled against discharge Q using the relationship proposed by Burbank et al. [2003] : $W = 0.01Q^{0.4}$. Dashed blue line is a power regression ($R^2 = 0.70$). Symbol type indicates the position inside the different swaths profiles of figure 1 in the main text. Symbol color indicates the bedrock geology of the catchment. The two largest catchments have been excluded. (B) Comparison between basin-averaged denudation rate and normalized channel steepness ($\theta_n = 0.45$). Like specific stream power, normalized channel steepness (ks_n) is dependent on stream morphology which incorporates influences of both climate and tectonics. For our dataset ks_n display an almost linearly relationship with denudation rates. Dashed blue line is a power regression ($R^2 = 0.67$). Same legend as previous inset. (C) Comparison between basin-averaged denudation rate and hillslope angle, which display the classical asymptotic behaviour associated with the occurrence of threshold hillslopes at high denudation rates [Ouimet et al., 2009]. Dashed blue line is the non-linear hillslope diffusion model of Roering et al. [1999], with the following parameters : critical hillslope angle $S_c = 28^\circ$, hillslope length $L_h = 100$ m, diffusion coefficient $D = 0.008$ m²/yr and rock- sediment density ratio $\beta = 2$. Same legend as previous inset. (D) Comparison between basin-averaged denudation rate and local or catchment relief. Local relief is measured over moving windows of 5 and 10 km diameter. These different measures of vertical development of topography are all positively correlated with denudation rates. (E) Comparison between basin-averaged denudation rate and catchment area, showing no correlation between our estimation of denudation and catchment size. (F) Comparison between the topographic metrics used in the previous insets and the actual primary tectonic (rock uplift rates from Lave ´ and Avouac [2001], red) and climatic (precipitation rates from Bookhagen and Burbank [2010], blue) forcings. Specific stream power, channel steepness and catchment relief display significant correlation with rock uplift rates, whereas the correlation with precipitation rates is weak or non-existent. The case of hillslope angles is more difficult to assess due to the existence of a stability threshold inducing a strong non-linearity in their response to different forcings.

References

- Arnold, M., Merchel, S., Bourlès, D. L., Braucher, R., Benedetti, L., Finkel, R. C., Aumaître, G., Gottsdang, A., and Klein, M. (2010). The french accelerator mass spectrometry facility aster: improved performance and developments. *Nuclear Instruments and Methods in Physics Research Section B: Beam Interactions with Materials and Atoms*, 268(11):1954–1959.
- Bookhagen, B. and Burbank, D. W. (2010). Toward a complete Himalayan hydrological budget: Spatiotemporal distribution of snowmelt and rainfall and their impact on river discharge. *Journal of Geophysical Research*, 115(F3):F03019.
- Bookhagen, B. and Strecker, M. R. (2012). Spatiotemporal trends in erosion rates across a pronounced rainfall gradient: Examples from the southern Central Andes. *Earth and Planetary Science Letters*, 327-328:97–110.
- Braucher, R., Brown, E. T., Bourlès, D. L., and Colin, F. (2003). In situ produced ^{10}Be measurements at great depths: implications for production rates by fast muons. *Earth and Planetary Science Letters*, 211(3-4):251–258.
- Braucher, R., Merchel, S., Borgomano, J., and Bourlès, D. (2011). Production of cosmogenic radionuclides at great depth: A multi element approach. *Earth and Planetary Science Letters*, 309(1-2):1–9.
- Brewer, I. D., Burbank, D. W., and Hodges, K. V. (2006). Downstream development of a detrital cooling-age signal: Insights from $^{40}\text{Ar}/^{39}\text{Ar}$ muscovite thermochronology in the Nepalese Himalaya. In Willett, S. D., Hovius, N., Brandon, M. T., and Fischer, D., editors, *Tectonics, Climate, and Landscape Evolution*, volume 398, pages 321–338. Geological Society of America Special Paper.
- Brown, E. T., Edmond, J. M., Raisbeck, G. M., Yiou, F., Kurz, M. D., and Brook, E. J. (1991). Examination of surface exposure ages of Antarctic moraines using in situ produced ^{10}Be and ^{26}Al . *Geochimica et Cosmochimica Acta*, 55(8):2269 – 2283.
- Burbank, D. W., Blythe, A. E., Putkonen, J., Pratt-Sitaula, B., Gabet, E., Oskin, M., Barros, A., and Ojha, T. P. (2003). Decoupling of erosion and precipitation in the Himalayas. *Nature*, 426(6967):652–655.
- Dunne, J., Elmore, D., and Muzikar, P. (1999). Scaling factors for the rates of production of cosmogenic nuclides for geometric shielding and attenuation at depth on sloped surfaces. *Geomorphology*, 27(1-2):3–11.
- Godard, V., Burbank, D. W., Bourlès, D. L., Bookhagen, B., Braucher, R., and Fisher, G. B. (2012). Impact of glacial erosion on ^{10}Be concentrations in fluvial sediments of the Marsyandi catchment, central Nepal. *Journal of Geophysical Research*, 117(F3):F03013.
- Lavé, J. and Avouac, J. P. (2001). Fluvial incision and tectonic uplift across the Himalayas of central Nepal. *Journal of Geophysical Research*, 106(B11):26561–26591.
- Nishiizumi, K., Imamura, M., Caffee, M. W., Southon, J. R., Finkel, R. C., and McAninch, J. (2007). Absolute calibration of ^{10}Be AMS standards. *Nuclear Instruments and Methods in Physics Research Section B: Beam Interactions with Materials and Atoms*, 258(2):403–413.
- Ouimet, W. B., Whipple, K. X., and Granger, D. E. (2009). Beyond threshold hillslopes: Channel adjustment to base-level fall in tectonically active mountain ranges. *Geology*, 37(7):579–582.
- Pratt-Sitaula, B., Burbank, D. W., Heimsath, A. M., Humphrey, N. F., Oskin, M., and Putkonen, J. (2011). Topographic control of asynchronous glacial advances: A case study from Annapurna, Nepal. *Geophysical Research Letters*, 38(24):L24502.
- Roering, J. J., Kirchner, J. W., and Dietrich, W. E. (1999). Evidence for nonlinear, diffusive sediment transport on hillslopes and implications for landscape morphology. *Water Resources Research*, 35(3):853–870.
- Scherler, D., Bookhagen, B., and Strecker, M. R. (2013). Tectonic control on ^{10}Be -derived erosion rates in the Garhwal Himalaya, India. *JGR*, in press.
- Seeber, L. and Gornitz, V. (1983). River profiles along the Himalayan arc as indicators of active tectonics. *Tectonophysics*, 92(4):335–367.

- Stone, J. O. (2000). Air pressure and cosmogenic isotope production. *Journal of Geophysical Research*, 105(B10):23753–23759.
- Whipple, K. X. and Tucker, G. E. (1999). Dynamics of the stream-power river incision model: Implications for height limits of mountain ranges, landscape response timescales, and research needs. *Journal of Geophysical Research*, 104(B8):17661–17674.
- Wobus, C., Whipple, K. X., Kirby, E., Snyder, N. P., Johnson, J., Spyropolou, K., Crosby, B., and Sheehan, D. (2006). Tectonics from topography: Procedures, promise, and pitfalls. *Geological Society of America Special Papers*, 398:55–74.